Alexandria Engineering Journal (2020) 59, 291–309

HOSTED BY

Alexandria University

Alexandria Engineering Journal

www.elsevier.com/locate/aej
www.sciencedirect.com

ORIGINAL ARTICLE

CFD characterization and optimization of the cavitation phenomenon in dredging centrifugal pumps

R. Ramirez [a], E. Avila [a], L. Lopez [a], A. Bula [b], J. Duarte Forero [a,*]

[a] Universidad del Atlántico, Departamento de Ingeniería Mecánica, Carrera 30 Número 8 – 49, Puerto Colombia, Área Metropolitana de Barranquilla, Colombia
[b] Universidad del Norte, Departamento de Ingeniería Mecánica, Km.5 Vía Puerto Colombia, Área Metropolitana de Barranquilla, Colombia

Received 6 January 2019; revised 1 December 2019; accepted 25 December 2019
Available online 5 January 2020

KEYWORDS

Cavitation;
Centrifugal pump;
CFD;
Dredging;
Slurry

Abstract A model has been developed to characterize the cavitation phenomenon in dredging centrifugal pumps. The operating parameters of a cutter type dredger: swing speed, dredging depth, and inclination, impeller rpm, as well as slurry characterizations such as density and velocity, are introduced, to determine how they influence the operation of the dredge pump. The geometric characterization of the hydraulic transport system of the dredger was performed. With the dredge operationaĺs parameters, along with the geometric characterization, the pump is modeled in CFD turbomachinery software. To validate the operational points, the CFD model considers the RNG k-ε model and the cavitating-multiphase flow. Through the central composite experiment design, the operating conditions range of the dredger is determined, in which the pump can operate and cavitate. This allows validating the model for different operational points. Finally, multiple regression shows the influence of each of the variables in the response obtained. Furthermore, the regression allows an understanding that operating conditions of the dredger must be adjusted to mitigate the phenomenon of cavitation in the dredging process.

1. Introduction

The dredging industry has provided a safe passage for ships across the world's oceanic channels [1]; thus, characterizing dredging operations to study the phenomena related to this activity requires high investment. A cutting suction dredge (DSC) is a floating platform equipped at one of its ends by a cutting device. The cutting head is mounted on the axis of the pipe suction, and its function is to disaggregate slurry from the bottom of the river to be suctioned by the centrifugal dredging pump through pipes to be deposited in barges [2]. A cutter suction dredger is divided into three subsystems: cutting, hydraulic slurry transportation, and finally, monitoring and control.

* Corresponding author.
E-mail address: jorgeduarte@mail.uniatlantico.edu.co (J. Duarte Forero).
Peer review under responsibility of Faculty of Engineering, Alexandria University.

https://doi.org/10.1016/j.aej.2019.12.041

Nomenclature

μ_m	mixture dynamic viscosity of the mixture [kg/m · s]
u	velocity [m/s]
p	pressure [Pa]
μ_t	turbulent viscosity [kg/m · s]
t	time [s]
δ_{ij}	Kronecker number [–]
i	unit vector [–]
j	unit vector [–]
k	unit vector [–]
f_v	mass fraction of vapor [–]
f_l	mass fraction of liquid [–]
f_s	mass fraction of solid [–]
R_e	vapor generation rate [kg/s]
R_c	vapor condensation rate [kg/s]
$\Re_B$	bubble radius [m]
C_e	constants in vapor generation rate [–]
C_c	constants in vapor condensation rate [–]
k	turbulence kinetic energy [m^2/s^2]
ε	turbulence dissipation rate [m^2/s^3]
P_k	shear production of turbulence [Pa]
$C_{1\varepsilon}$	$k-\varepsilon$ turbulence model constant [–]
$C_{2\varepsilon}$	$k-\varepsilon$ turbulence model constant [–]
C_μ	$k-\varepsilon$ turbulence model constant [–]
σ_k	turbulence model constant for the k equation [–]
σ_ε	turbulence model constant [–]
P_s	suction pressure [Pa]
P_d	discharge pressure [Pa]
g	gravity vector [m/s^2]
Z_1	depth of dredging [m]
p_{vap}	vapor pressure [Pa]
TDH	total dynamic head of slurry [m]
$NPSH_a$	net positive suction head admissible of slurry [m]
NPSHr	net positive suction head requerid of slurry [m]
RPM	revolutions per minute [min^{-1}]
ρ_m	density of mixture [kg/m^3], [ton/m^3]
ρ_v	density of vapor [kg/m^3]
ρ_l	density of liquid [kg/m^3]
ρ_s	density of solid [kg/m^3]
$\propto_v$	vapor volumetric fraction [–]
$\propto_l$	liquid volumetric fraction [–]
$\propto_s$	solid volumetric fraction [–]
λ	surface tension [N/m]
ρ_{md}	density of slurry [kg/m^3]
CCL	CFD command language
$VACUUM_{admissible}$	vacuum admisible [in Hg]

Since the cutter type dredger can perform both excavation and sediment transport at the same time, its performance is much better than other types of dredgers. What makes control tasks more complex is that many factors, which have a significant impact on the dredging process, cannot be measured, or they are obtained with little precision [3]. This results in fierce competition from contractors involved in dredging projects, looking for a better performance of control operations [4].

The pump is the heart of any hydraulic transport system because it establishes both the performance and reliability of the system. Today, a wide range of sediment pumps are available in the market, where the centrifugal type is the most useful in the transport of suspended solids because they are the best fit to work in applications of high volume and low elevation [5]. Due to this advantage, the centrifugal pumps in the dredging industry cover a wide range of services operating far from their design area [6] and are subject to flow variations [7], generating cavitation problems. The need to mitigate the negative effects of the cavitation on the part of dredger operators results in excessive demand of time.

Slurry transport control is another important aspect of the dredging process. For this purpose, the cutting of the soil is mixed with water and then introduced into the pipe. It is good to point out that the problems of pressure losses caused by the transport of typical suspensions through a centrifugal dredging pump are of special interest given the high powers being handled [8].

In recent years, the growing availability of computational sources and progress in the accuracy of numerical methods has helped researchers to solve turbomachinery problems for industrial markets [9]. CFD complements testing and experimentation, reducing the efforts and costs required for experimental procedures and data acquisition [10].

From the literature review, it is noticed that cavitation is the most relevant hydrodynamic phenomenon associated with fluids transportation [11]. Cavitation occurs when the fluid reaches the local vapor pressure forming cavities; these cavities or bubbles travel to areas of greater pressure and implode, producing shock waves [12]. If the collapsing bubble is close to a metal surface, it will cause cyclic stress due to continuous implosions [13]. For this reason, the collapsing dynamics are complex and depend on a variety of factors, including surface tensions, viscous effects, and non-condensable content [14].

The prediction of cavitation inception and performance in centrifugal pumps is important for engineering applications [15]. Pumps are widely applied in various industries, under this premise the cavitation in the pumps has allowed introducing many concepts such as NPSH, cavitation number, the turbulent viscosity and the utilization of visual measurement instruments with the final purpose to evaluate the operation condition.

As expected, there are no models for cavitation that try to account for all these complexities, such as multiphase, phase change, compressibility, and turbulence. However, some models take into account the effects of non-equilibrium; many of these models are based on the Rayleigh-Plesset equation [16], which describes the growth and collapse of a single bubble subject to pressure shocks [17]. Limbach [18] present three-dimensional (3D) simulations with ANSYS, as well as measurements of the cavitating flow in a low specific speed centrifugal pump (nq = 12 min^{-1}) and study the performed for different operating conditions and varying surface roughness. Zhang [19] investigated by numerical and experimental methods the cavitation in centrifugal charging pumps (CCPs) in nuclear power plants. In this study, the cavitation-induced unsteady flow characteristics of a CPR1000 CCP and the

absolute error between the simulated and measured NPSHr was 3.6%, and that between the calculated and measured head was 2.9%, validating the simulation of the cavitation performances of a CCP.

It is important to note that many of the cavitating flows are also turbulent, so the choice of the turbulence model in numerical predictions of cavitating flows is of great importance and care [20]. Thus, turbulence models such as Reynolds-Averaged Navier Stokes (RANS) [21] and k–ε EARSM [22] have been adopted to simulate cavitation in turbulent flows. In this way, the present article is mainly concerned with the cavitation study grounded in the prediction techniques and modeling of the rotating frame. A Filter-Based Model (FBM) based on the RNG k–ε model, and a modified Zwart model are adopted by Liu et al. [22] to model the unsteady cavitating flows in the pump, the analysis results represent truly the development of the attached sheet cavitation in the impeller and the positive development of the performance in centrifugal pumps.

Meshing techniques for transient flow simulations in centrifugal pumps [23] have been carried out, which illustrates the superiority of sliding meshing techniques in computational efficiency and the configuration of the different rotational and stationary frames. Courtier-Delgosha [24] presented a special test performed to double curvature blades pump, to investigate cavitation under multiple models. The code was generated in FINE/TURBOTM Software, as well as the numerical and experimental results concerning the pump characteristics were compared in different flow conditions.

Critical meshing techniques, such as tetrahedral mesh with hexahedral elements in the center, were implemented by Li [25], under stepwise discretization scheme and mesh adaptation, to ensure that the computational numerical process was stable and precise. In this way, the cavitation model was validated against the experimental data, along with a comparison with the NPSHr correction factor estimated with the empirical correlation curve and the experimental results achieved.

The CFD analysis has not only been used for the direct analysis of cavitation, but it has also been used in other systems, such as the study of Searaser which may be capable of being used in the Caspian Sea, demonstrating that the results thrown by the simulations showed good agreement as the experimental data [26].

Although it is true that the equations implemented in the dredging equipment by Wilson [27] and the analysis made by Miedema et al. [28] provide an adequate level of understanding of a sediment transport system, it is clear that for realistic Reynolds numbers and turbulence, direct numerical solutions (DNS) of this flow will require a computing power far superior to that currently available in the dredging industry.

The main objective of this research is to develop a predictive model to characterize the cavitation phenomenon in centrifugal pumps applied to dredge and to find the influence of each one of the variables of operation of the dredger. The importance and relevance of the present modeling of the cavitation allow us to identify in a certain moment the durability of the components of the dredging pump and to identify the influence that the modeling of this phenomenon has in this turbomachinery in the operating parameters controlled by the operator in the dredge.

2. Mathematical modeling

For purposes of carrying out a practical and general model of flows with the presence of the cavitation phenomenon, we considered the particle transport model or Lagrangian-Eulerian approach capable of modeling the dispersed phases that are discretely distributed in a continuous phase [23]. The implementation of the particle transport modeling in CFD used is considered as a multiphase flow in which the particles are a dispersed phase. The Lagrangian model adopts the dispersed phase, while all other phases are considered continuous or Eulerian. In the dispersed phase, the entrained particles interact with the fluid and other particles discretely [29].

The study carried out to select which multiphase model was based on the fact that under adverse conditions of the river, the fluid phase is treated as a continuous phase while the dispersed phase that is to say the second occupied a low volumetric fraction compared to the large mass load. Through this concept, the particle trajectories are solved individually at specific intervals during the calculation of the fluid phase. This makes the model of liquid-liquid mixtures and any application where the volumetric ratio with respect to the concentration is not so impressive in the internal approach of multiphase flow dynamics.

By establishing a suitable turbulence model for the characterization of cavitation in multiphase flows such as the present one, four criteria are established: what is adopted by the literature, the physical nature of the problem, the quality of the expected results, and finally, computational requirement that entailed the current characterization of the cavitation phenomenon. According to this, the fluids in the cavitation flow field for the pumps are considered as a homogeneous mixture [30] and compressible vapor and liquid. For the present study, the continuous phase is assumed to be turbulent, and therefore, effective viscosity is computed using the turbulence models in the subsequent sections are discussed. The$i$, j and k denote the directions of the axes. Thus, the equations of momentum and continuity in cartesian coordinates are as follows:

$$\frac{\partial \rho_m}{\partial t} + \frac{\partial (\rho_m u_i)}{\partial x_i} = 0 \tag{1}$$

$$\frac{\partial (\rho_m u_i)}{\partial t} + \frac{\partial (\rho_m u_i u_j)}{\partial x_j} = -\frac{\partial p}{\partial x_i} + \frac{\partial}{\partial x_j}\left[(\mu_m + \mu_t)\left(\frac{\partial u_i}{\partial x_j} + \frac{\partial u_j}{\partial x_i} - \frac{2}{3}\frac{\partial u_k}{\partial x_k}\delta_{ij}\right)\right] \tag{2}$$

where $\boldsymbol{u}$ is the velocity, p is the pressure and μ_t is the turbulent viscosity, t is the time and $\delta_{ij}$is the Kronecker number, respectively. It is important to highlight the consideration in the two-fluid approach; it is assumed that both fluids/phases share the same pressure field [31]. μ_m and ρ_m are the dynamic viscosity and density of the mixture, calculated by the average weight of each volumetric fraction as follows:

$$\mu_m = \propto_v \mu_v + \propto_l \mu_l + \propto_s \mu_s \tag{3}$$

$$\frac{1}{\rho_m} = \frac{f_v}{\rho_v} + \frac{f_l}{\rho_l} + \frac{f_s}{\rho_s} \tag{4}$$

$$f_v = \frac{\propto_v \rho_v}{\rho_m} \tag{5}$$

$$f_l = \frac{\propto_l \rho_l}{\rho_m} \tag{6}$$

$$f_s = \frac{\propto_s \rho_s}{\rho_m} = 1 - f_v - f_l \tag{7}$$

where $\propto_v, \propto_l$ and $\propto_s$ are the volumetric fractions of the components. f_v, f_l and f_s are the mass fractions of the components of steam, liquid, and pumped particles. ρ_v, ρ_l and ρ_s are the densities of the components. μ_v, μ_l and μ_s are the viscosity of steam, liquid, and pumped particles, respectively.

On the other hand, in most engineering devices, low-pressure regions, where cavitation occurs, are also regions of relatively high velocities. In such high-speed regions, the velocity oscillations between the liquid and vapor phases are rather small. Unfortunately, there are no general or reliable physical models for these parameters, and therefore the additional computational effort in the two-fluid approach is of little practical value.

In this way, the present model concentrates on the use of simple and rational expressions for the rates of phase change. From this perspective the vapor mass fraction f_v, is governed by the transport equation:

$$\frac{\partial(f_v \rho_m)}{\partial t} + \nabla \cdot (\propto_v \rho_v u) = R_e - R_c \tag{8}$$

where the terms R_e and R_c denote steam generation and condensation ratio, and maybe functions of flow parameters, pressures, characteristic flow velocity, liquid and vapor phase densities, saturation pressure, and liquid-vapor surface tension.

The sedimentological condition analysis was based on an appropriate standard of the granulometric composition of the riverbed in Calamar [32]. It was observed that the D50 sizes of the sediments of the Canal del Dique vary between fine silt and very fine sand (0.008–0.125) when compared with the classification according to material sizes the spatial distribution of the sediment concentration constitutes an approximation to the morphological behavior, in this sector, the average total concentration of sediments in measured suspension (Ct) and the average concentration of sand in measured suspension (Ca) mean a low concentration and therefore a low volumetric fraction in the dispersed phase that varies little, or it will be taken as insignificant [33].

2.1. Effect of bubble dynamics

In most engineering situations, there are a variety of forms of core creation for the initiation of cavitation. Therefore, the main focus is to take into account an adequate understanding of the particular growth of the bubble and collapse. In a fluid flowing with zero slip velocity between the fluid and the bubbles [14], the bubble dynamics equation can be derived from the generalized Rayleigh-Plesset equation:

$$\Re_B \frac{D^2 \Re_B}{Dt^2} + \frac{3}{2}\left(\frac{D^2 \Re_B}{Dt^2}\right)^2 = \left(\frac{P_B - P}{\rho_l}\right) - \frac{4 v_l}{\Re_B}\dot{\Re}_B - \frac{2S}{\rho_l \Re_B} \tag{9}$$

This equation implements a physical approach to introduce the effects of bubble dynamics on the cavitation model. Thus, to obtain an expression of the net change rate of phase, it is modified from [31] to obtain the ratio of the density of the mixture and the vapor fraction $\propto_v$:

$$\frac{D\rho}{Dt} = -(\rho_l - \rho_v - \rho_s)\frac{D\propto_v}{Dt} \tag{10}$$

The vapor fraction $\propto_v$ is related to the bubble number density "n" (a number of bubbles per unit of volume in the flow) and the radius of the bubble $\Re_B$ as:

$$\propto_v = n\frac{4}{3}\pi \Re_B^3 \tag{11}$$

Using the Rayleigh-Plesset equation without the second and third term on the right side and combining equations (1), (5), (7), (8), (9), we finally obtain the expression for the phase change Re regarding radius of the bubble $\Re_B$:

$$R_e = \frac{3 \propto}{\Re_B} \cdot \frac{\rho_v \rho_l}{\rho}\left[\frac{2}{3}\frac{P_v - P}{\rho_l}\right]^{\frac{1}{2}} \tag{12}$$

In this way and using arguments of Si [23], which indicates the fact that the phase change must be proportional to the change of volumetric fraction, the following expressions are obtained:

$$R_e = C_e \frac{\sqrt{k}}{\lambda}\rho_l \rho_v \left[\frac{2}{3}\frac{p_v - p}{\rho_1}\right]^{\frac{1}{2}}(1 - f_v - f_l) \tag{13}$$

$$R_c = C_c \frac{\sqrt{k}}{\lambda}\rho_l \rho_l \left[\frac{2}{3}\frac{p_v - p}{\rho_1}\right]^{\frac{1}{2}} f_v \tag{14}$$

where the empirical factors are $C_e = 0.02$ y $C_c = 0.01$, gas mass fractions $f_l = 1.5 \cdot 10^{-5}$, the coefficient of surface tension $\lambda = 0.0717$ N/m, p_v denotes the vaporization pressure, and k denotes turbulent kinetic energy.

2.2. Effect of the turbulence model

In general, two equations turbulence models are adopted due to their simplicity and lower computational requirements [22]. The quality of the initial results obtained from models such as k-ε, k-ω, and RSM, was poor, and there were problems to attain convergence, even at large computational time.

This evidence, together with the authors' arguments, points out that the mathematical considerations of the previously mentioned models are derived from non-cavitating flows, which restricts to some extent, these models [21]. A substantial improvement in results, the model RNG k-ε, which is a robust model coming from improvements and modifications in the k-ε model considerations [34].

CFD allowed formulating the dispersed phase sufficiently diluted so that the interactions between particles and the effects of the fraction of volume of particles in the gas phase are insignificant, taking into account the bubbles product of cavitation. Important to note that the interaction between the solid particles and the liquid phase can be carried out from relative monitoring of them since they are traced from an absolute frame through the non-deformation of meshes. Thus, in dredging practice, these problems imply that the discrete phase must be present in a fairly low volume fraction, generally less than 10–12%.

The turbulence model RNG $k - \varepsilon$, which makes corrections of the coefficients in the equation of the standard turbulence model $k - \varepsilon$, and can better predict the rotational flows, as follows:

$$\frac{\partial(\rho_m k)}{\partial t}+\frac{\partial(\rho_m k u_i)}{\partial x_i}=P_k-\rho_m\varepsilon+\frac{\partial}{\partial x_j}\left[(\mu_m+\frac{\mu_t}{\sigma_k})\frac{\partial k}{\partial x_j}\right] \quad (15)$$

$$\frac{\partial(\rho_m \varepsilon)}{\partial t}+\frac{\partial(\rho_m \varepsilon u_i)}{\partial x_i}=C_{1\varepsilon}\frac{\varepsilon}{k}P_k-C_{2\varepsilon}\rho_m\frac{\varepsilon^2}{k}+\frac{\partial}{\partial x_j}\left[(\mu_m+\frac{\mu_t}{\sigma_\varepsilon})\frac{\partial \varepsilon}{\partial x_j}\right] \quad (16)$$

$$\mu_t=\rho_m C_\mu\frac{k^2}{\varepsilon} \quad (17)$$

where k and ε are the kinetic energy of the turbulence and the rate of dissipation, P_k is the production of turbulence due to viscous forces, σ_k and σ_ε are the turbulent Prandtl numbers for$k$ y ε, respectively. The following parameters were defined for the model constants $C_{1\varepsilon}$, $C_{2\varepsilon}$, C_μ, σ_k y σ_ε: $C_{1\varepsilon}=1.42$, $C_{2\varepsilon}=1.68$, $C_\mu=0.0845$, $\sigma_k=0.7179$ y $\sigma_\varepsilon=1.42$, based on research by other authors [24].

2.3. Geometry and operational parameters of the dredger cutting Rio Magdalena

Rio Magdalena dredger is a self-propelled dredger, with excellent maneuverability in the dredging operations to maintain the navigable depth in the waterways of Calamar, this dredger is illustrated in Fig. 1.

The dredger has a maximum dredging depth of 13 m, operating on the average fine sand with a mean grain size d_{50} = 0.169 mm [37]. The dredge moves the material along 33 m of the suction pipe, having 0.61 m in diameter (24 in.). Approximately 15 m are submerged. Other specifications of the dredger can be found in Table 1.

The Rio Magdalena dredge relies onboard instrumentation to provide and collect data on operating parameters such as cutter speed, swing speed, pressure at different positions, engine what drives the pump in revolutions per minute, depth and pitch of the suction line, and slurry characteristics such as velocity and density; which influence the operation of the dredge pump. The analysis parameters of the dredging are shown in Fig. 2.

The point where the slurry enters and that connects with the pump suction through a flexible joint, moves from one side to the other at the bottom of the river, to cover a wide dredging surface. The speed at which it moves is what is known as swing speed (Fig. 2b). Increasing this speed decreases the dredging efficiency since the cutting tip does not raise enough slurry.

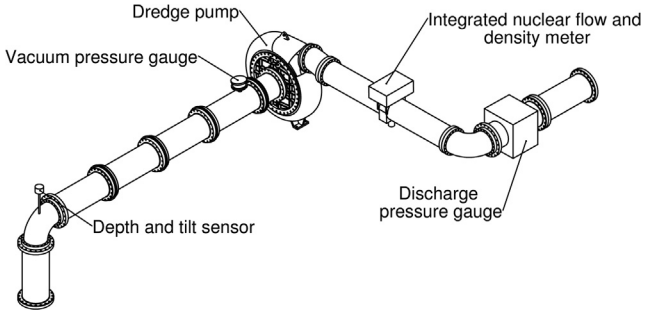

Fig. 1 Description of the hydraulic transport system instrumentation.

Table 1 Specifications of the Rio Magdalena dredger.

Strut [m]	2.70
Maximum draft [m]	1.20
Suction pipe diameter [m, in]	0.61, 24
Discharge pipe diameter [m, in]	0.61, 24
Maximum depth of dredging [m]	13
Power in the cutter [kW]	500

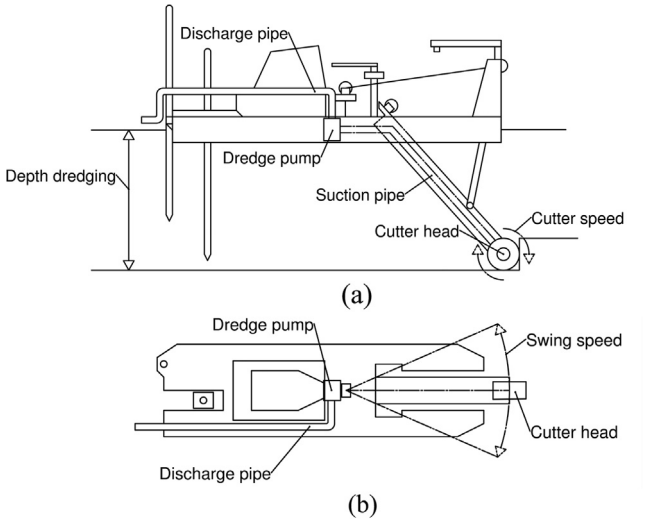

Fig. 2 Analysis parameters of a Cutter Suction Dredger: (a) side view and (b) top view.

Dredger nuclear density meters (DHMART) operate on the principle that gamma radiation emitted by a radioactive isotope is absorbed by both water and sand. The detector accurately measures the level of radiation that passes through the suspension, which changes with the density of the suspension, and converts that measurement to a specific density or gravity. Fig. 1 provides a schematic of the instruments and the suitability of each of these in the hydraulic transport system. The operation is directed from the control cabin, and the data obtained in the field is observed in Table 2.

3. CFD simulation methodology and definition of parameters

The fact that the current characterization was affected by geometric and operational parameters of the dredge, and fluid characterizations, involved the creation of variables, expressions, and functions with the CFD model was controlled with input parameters, is reflected using software: characterization of the dredging process from a programming language within the simulation.

3.1. Creation of geometry/meshing

The simulated centrifugal pump is a single inlet, with a closed three blades impeller of 1750 mm in diameter. The objective was to produce a mesh that would fit the physics and geometry. During the simulation configuration, boundary conditions

Table 2 Experimental record of operation data of the dredger.

Parameters and operation constants	Units	Test 1	Test 2	Test 3
Suction pipeline length	[m]	32.68	32.68	32.67
Discharge pipeline length	[m]	45.00	45.00	45.00
Cutter revolutions	[rpm]	15.00	15.00	14.99
Cutter speed	[m/s]	1.18	1.18	1.18
Engine revolutions	[rpm]	732.00	724.00	728.00
Reducer plate	[-]	3.48	3.48	3.48
Impeller angular speed	[rpm]	213.22	208.05	209.20
Suction pressure	[Pa]	67727.81	63568.63	54182.24
Discharge pressure	[Pa]	242502.53	239330.47	230135.08
Tilf angle suction pipeline	[°]	24.99	31.39	36.13
Depth of dredging	[m]	6.70	8.26	9.35
Slurry volumetric flow	[m^3/s]	1.17	1.42	1.82
Swing speed	[m/s]	0.11	0.13	0.20
Density	[ton/m^3]	1.20	1.30	1.50
Slurry velocity at the discharge	[m/s]	4.00	4.50	5.00
Slurry mass flow	[kg/s]	1400.95	1707.40	2188.98

and regions of interest were defined for the specific physical phenomenon, indicated in Fig. 3.

The generation process has considerable control over the distribution of the mesh elements to minimize computer resources and take advantage of the flow passage. To ensure that the best mesh for the solution is obtained, a general meshing control was established, an overall adjustment was made in the meshing strategy, mesh type to be generated, size and relevance of the elements, and inflation in strategic places like the blades of the impeller. Due to the complexity of the computational domains, that is to say, an unstructured hexahedron in impeller and tetrahedron in the pipe was adopted because of its fine adaptability. In the near-wall region, a fine mesh is required for RNG k-ε, so the mesh near to the wall is refined. When the mesh quality criteria fall within the correct range, the mesh was validated first based on the mesh metrics to Table 3 and the results accepted by the Solver of Statistical criteria (Table 4).

Finally, the solution found in important details of geometry was excellently captured without convergence problems, such as the curvatures in the three blades, the predominant curvature of the scroll, and the objective connections or interfaces.

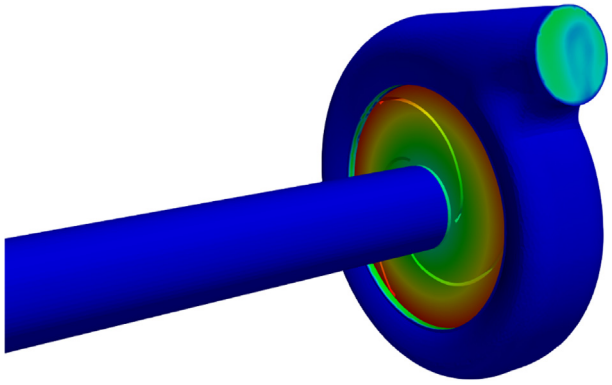

Fig. 3 Region of interest for Meshing, contact objective: Impeller-volute.

The solution has converged to a steady value for our values of interest that, for this case, pressure and mass flow.

It is important to note that different CFD solvers and physics have different requirements for mesh quality. Finally, the characteristics of nodes, elements, and their respective statistical values obtained in Table 3. In this way, the mesh for the characterization of the phenomenon of cavitation in centrifugal pumps applied to the dredging counts with excellent values for both the relation of symmetry (Skewness) and orthogonal quality (Orthogonal Quality) indicated in the Fig. 4 by the meshing approach to the different 3D cell types that the method assignment: tetrahedral (Tex4), pyramidal (Mex5) and prismatic (Wed6).

3.2. Definition of the physics of the model

The mesh of the pump was obtained using the refinement from the previous process. All physical considerations involved in the simulation at this stage, the definition of the working fluid, and the appropriate boundary conditions and interfaces.

3.2.1. Domain

This model includes three domains or regions of the fluid flow: the inlet pipe, the passage of the flow between the three blades impeller and the fluid present in the volute, and the simulation were performed under steady-state conditions.

3.2.2. Frame

Given the movement of the impeller blades relative to the volute and stationary pipe, the analysis involved multiple frames of reference. A rotating reference frame is imposed for the impeller domain, while the fluid inside the pipe and the volute are established in a stationary reference frame.

3.2.3. Boundary conditions

It was important to establish boundary conditions that accurately reflected the actual situation and provided acceptable results in pump simulation. Is recommend some appropriate configurations [30], depending on the criterion of convergence and robustness of the results. The total pressure was estab-

Table 3 Statistics and mesh metrics.

Metric and mesh statistics	Relationship of asymmetry	Orthogonal quality	Quality of the element	Aspect Ratio
Minimum	1.51E-04	0.176	0.128	10.266
Maximum	0.787	0.999	0.999	9.452
Average	0.158	0.923	0.877	1.260
Standard deviation	0.113	8.28E-02	8.87E-02	0.109
Nodes	942,435			
Elements	1,755,523			

Table 4 Statistical criteria accepted by CFD-Solver.

Mesh statistics						
Domain Name	Orthogonality angle		Expansion factor		Aspect ratio	
Impeler	26.41	Acceptable	34	Acceptable	9	Good
Pipeline	59.92	Good	6	Acceptable	8	Good
Case	45.60	Acceptable	10	Acceptable	6	Good
Global	26.44	Acceptable	34	Acceptable	9	Good

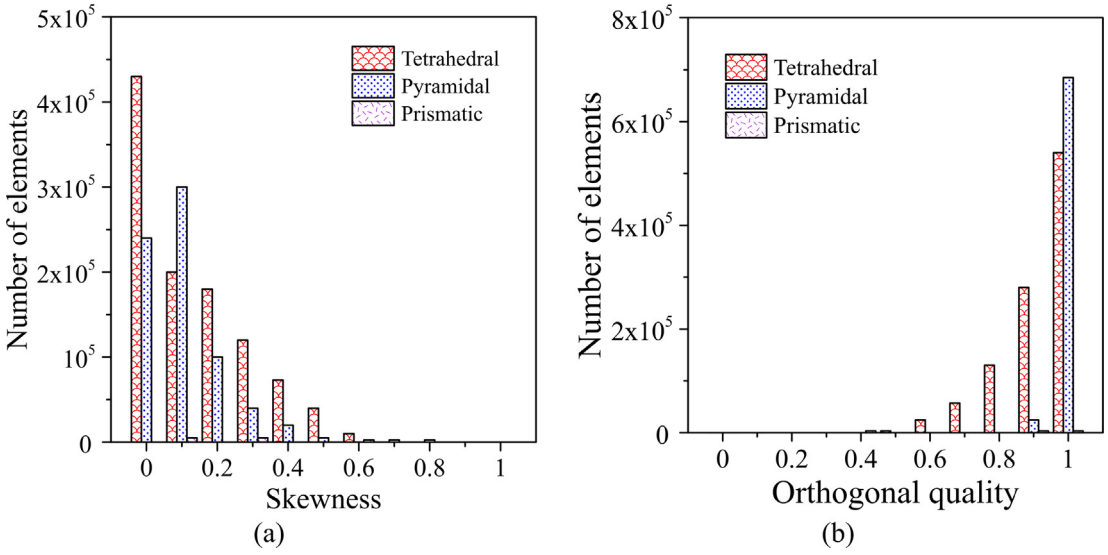

Fig. 4 Mesh Quality Metric Graph: (a) Skewness and (b) Orthogonal quality.

lished at the inlet of the pipe with a turbulent intensity of 5% and mass flow at the outlet of the volute. Likewise, non-slip conditions were imposed on the walls and the impeller blades, as well as wall conditions on the volute.

3.2.4. Multiphase Eulerian-Lagrangian

Two fluids are used in the computational domain, performing the coupling of the particles or slurry with an average diameter of 0.16 mm and 1. Particle-particle interactions are modeled using kinetic theory. The drag, the lift, near-wall, and turbulent dispersion forces were implemented [34].

3.2.5. Turbulence and treatment near walls

The turbulence model RNG k-ε was adopted for the simulation along with a homogeneous multiphase model. Likewise, in regions near the wall, there are very high gradients of quantities involved in the analysis and, therefore, require special attention. Scalable wall functions overcame one of the major drawbacks of the standard wall feature approach, allowing for reduced computational stresses and improved near-wall results.

3.2.6. Interface domain

For the development of the simulation, which presented two frames of reference, two models were applied: the general interface connection and the GGI or General interface model. This is required due to different mesh densities between the scroll and the impeller. This allows for obtaining steady-state predictions for turbomachines [30].

4. Characteristic performance and cavitation condition of the centrifugal pump

The established solution criteria can be observed in Table 5, so the simulations were started, establishing a final CFD language, a monitor of runs, and criteria for monitoring the variables. The high-resolution scheme (HRS) was used for the advection terms as for the equations of the turbulence model [31].

Table 5 shows the solution criteria set up for the simulation. A high-resolution scheme (HRS) for the advection terms as for the equations of the turbulence model [34] was established. The High-Resolution transient scheme uses the second-order backward Euler scheme wherever and whenever possible and reverts to the first-order backward Euler scheme when required to maintain a bounded solution [28].

The discretized conservation equations of mass, momentum was simultaneously coupled and solved using double precision in the calculation. For the normalized sum of the residuals of the discretized equations, a convergence criterion of 10^{-4} was

Table 5 Solution criteria.

Solver Control		*Convergence Criteria*	
Advection Scheme	High Resolution	Residual type	RMS
Turbulence	High	Residual	1.00E−04
Numeric	Resolution	Target	

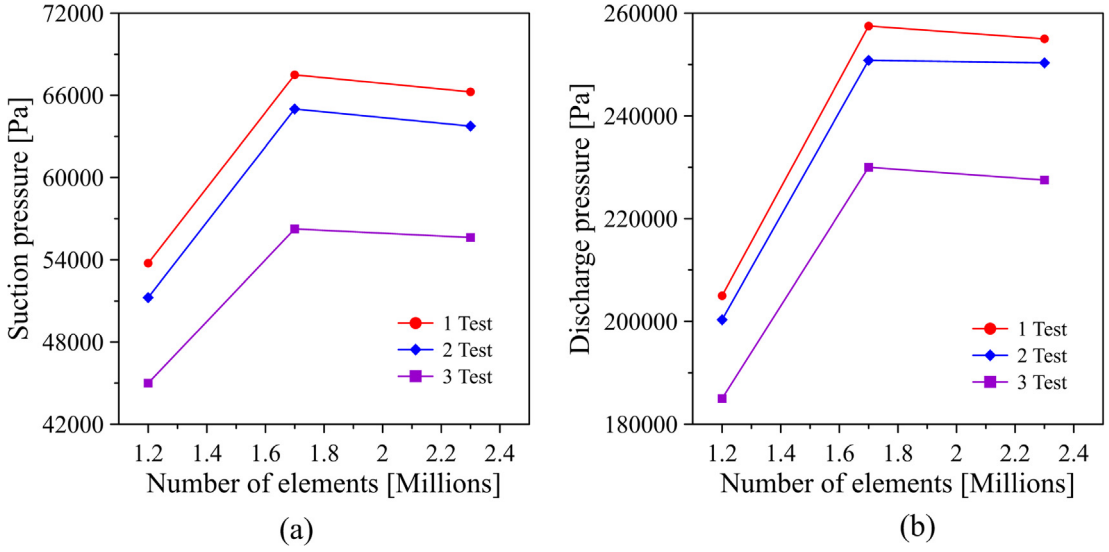

Fig. 5 Mesh independence study for resultant monitor value of (a) suction and (b) discharge pressure.

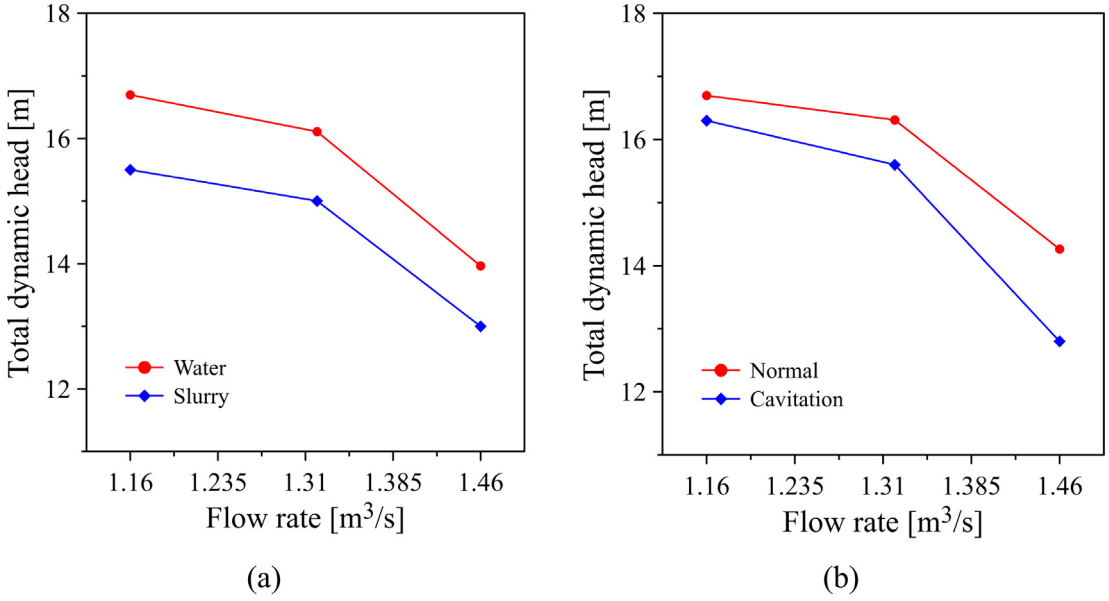

Fig. 6 (a) Effect of slurry and (b) effect of cavitation on the total dynamic head.

considered. The residual is a measure of the local imbalance of each conservative control volume equation and is the most important measure of convergence as it relates directly to whether the equations solved accurately. With the extensive literature review, it was found that many authors describe meshing independence qualitatively [17,25], and this approach was followed to establish mesh independence, and it is presented in Table 5.

The mesh independence check was carefully carried out for each approach before analyzing the simulation results. For each point of the simulation, the following was ensured: the residual root means square (RMS) error converged to 10^{-4}, the monitor points for pressures of interest were repeatable, and the domain imbalance was far below 2%. Finally, three different meshes are used to satisfy the grid requirements for the three near-wall solution approaches. A mesh with a total of 1,755,523 elements or cells was utilized as the best compromise between solution-accuracy requirements and computational resources, as shown in Fig. 5, for a time of 20 h for each of the three tests.

For test 1, test 2 and test 3, the slurry density was set at 1.20, 1.30, and 1.50 ton /m^3, and the flow rate at 1400.95, 1707.40, and 2188.48 kg/s. The angular velocity of the impeller was kept constant at 210 rpm for all three tests. The other parameters taken into account in the tests are detailed in Table 2.

The total dynamic head (TDH) of the dredging pump changes due to the coupling effect between the solid and liquid phases. Fig. 6.a show this effect for various flow conditions. It is observed that slurry causes an average reduction in TDH of 8% when compared to water. In the investigation of Li et al. [39], similar results were obtained.

In addition, the impact of cavitation on the dredging pump was evaluated. The results are shown in Fig. 6b. As expected, cavitation leads to a reduction in pump TDH. This reduction increases gradually as the pump flow increases. For the flow

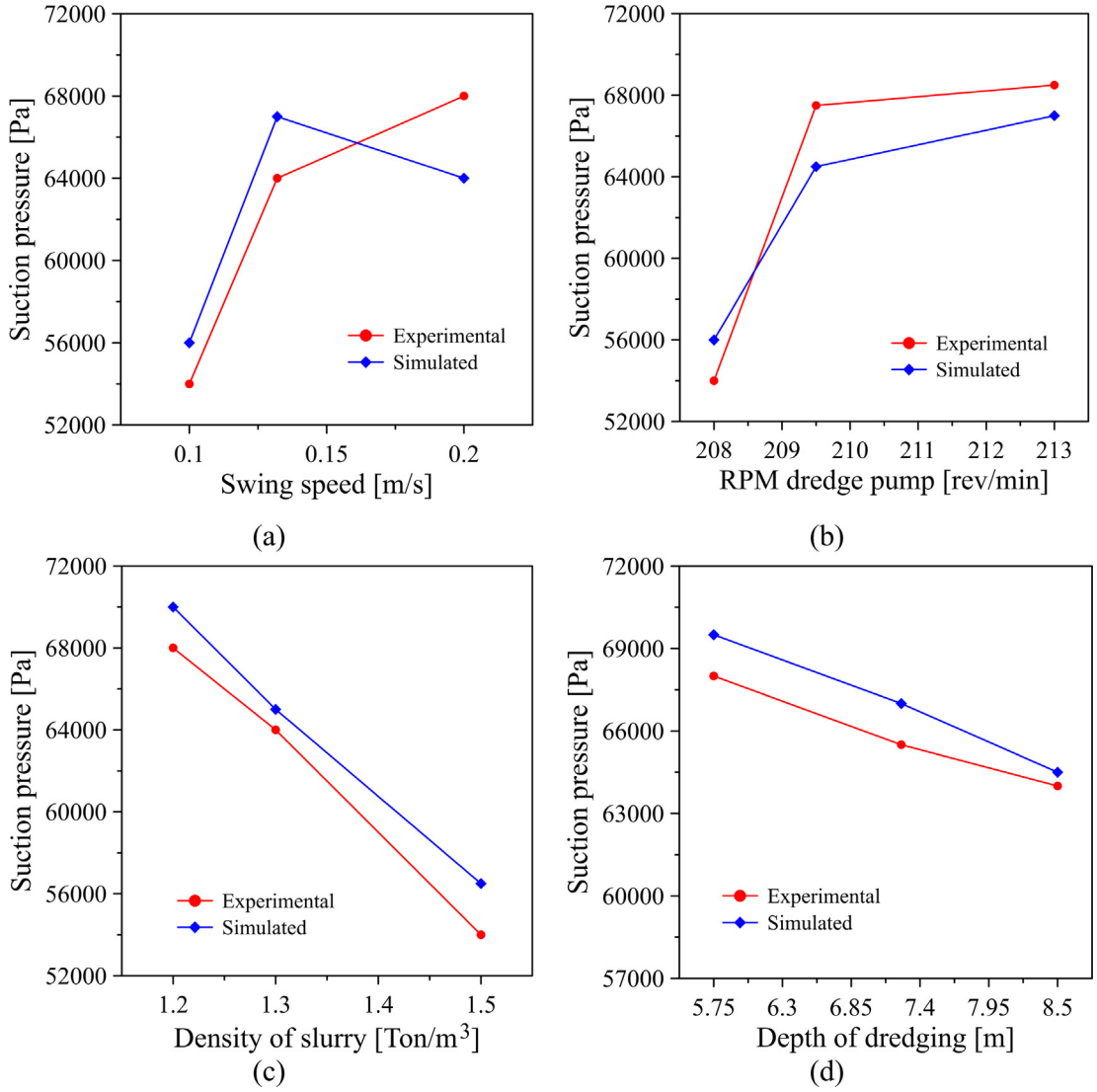

Fig. 7 Comparison of simulated versus experimental results of suction pressure concerning the operating variables of the dredge: (a) swing speed, (b) RPM, (c) density of slurry, and (d) depth of dredging.

conditions studied, the average reduction was 5.66% when compared to normal operating conditions.

Finally, to have a greater amount of information without gathering data from the field, a validation process was carried out through the analysis of the performance characteristic using simulated results along with experimental data. The pump performance is compared to variables obtained from the monitoring system, i.e., pump inlet and outlet pressure. The experimental pressure values obtained at the pipe suction and discharge, which were acquired in this research, were also compared with those obtained in the CFD simulations, as shown in Figs. 7 and 8.

The results in Figs. 7 and 8 show that the increase in suspension density results in a decrease in pump suction and discharge pressure. This is attributed to the increase in pressure drop caused by the increase in fluid density. Additionally, the increase in the number of solid particles in the fluid causes an increase in the kinetic turbulence energy of the fluid, thus increasing the energy needed to pump the slurry into the pump. Zhao and Zhao [40], and Li et al. [39] report similar results for the pressure behavior of the dredging pump.

The increase in dredging depth also caused a reduction in the suction and discharge pressure of the pump. The pressure drop is attributed to the increase in head loss, caused by the more abrupt change in direction experienced by the flow as the suction pipe forms a right angle to the water surface.

The distribution of pressures and the trajectories of the fluid along the hydraulic system are by the low-pressure contours of the system configurations regarding meshing (Fig. 9).

Based directly on the measurements carried out, the head of the dredge pump and the NPSHr are defined as:

$$TDH_{slurry} = \frac{P_d - P_s}{\rho_{md} \cdot g} \tag{18}$$

$$NPSHr = C_t \cdot N^{\frac{4}{3}} \cdot Q^{\frac{2}{3}} \tag{19}$$

where C_t, N and Q are the hydraulic coefficients for centrifugal pumps ($C_t = 0.0011$) [41], pump rotor rotation number and flow rate.

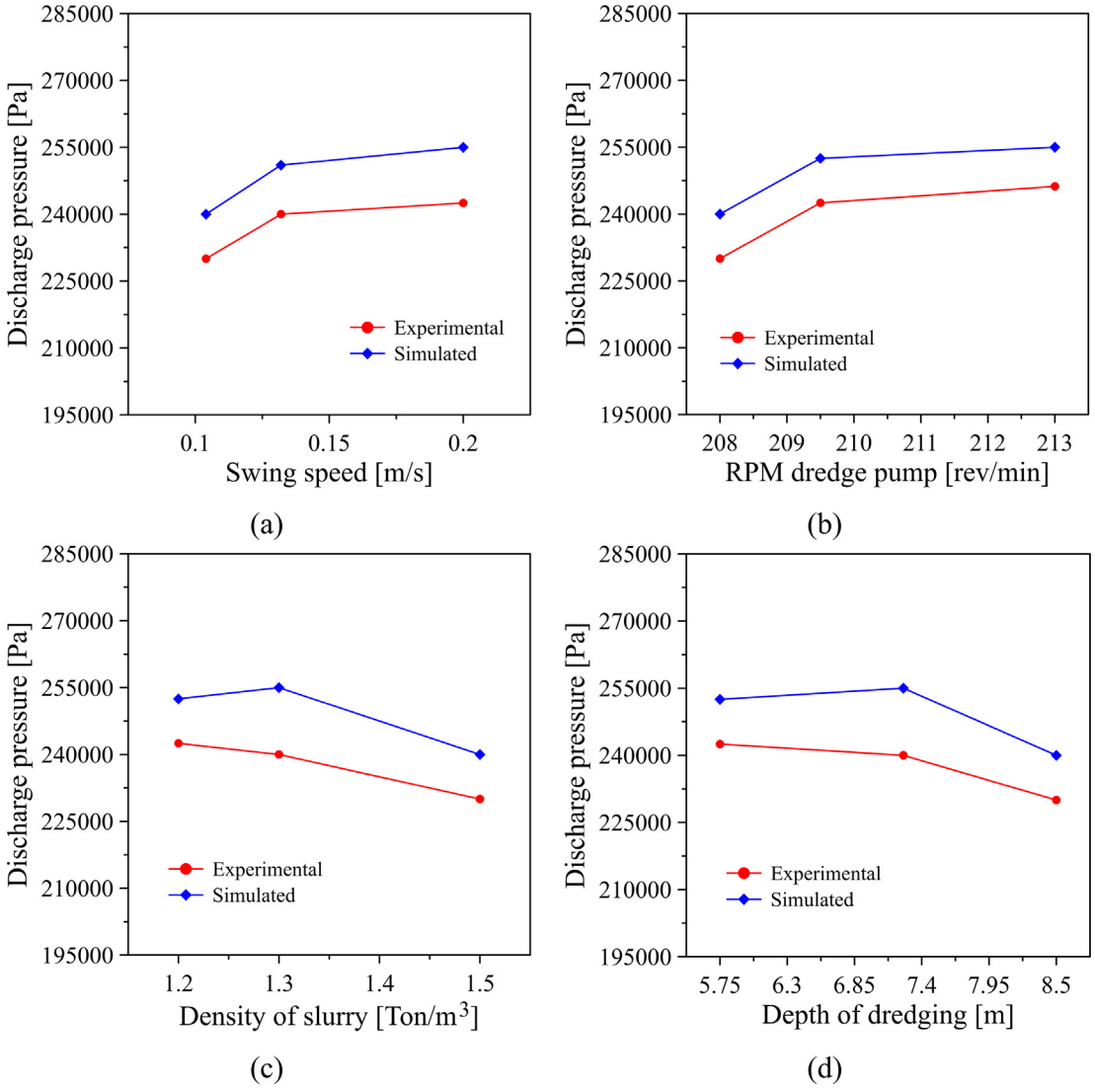

Fig. 8 Comparison of simulated versus experimental results of discharge pressure concerning the operating variables of the dredge: (a) swing speed, (b) RPM, (c) density of slurry, and (d) depth of dredging.

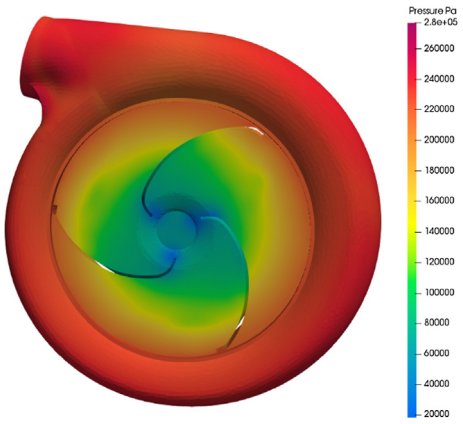

Fig. 9 Pressure gradients in the pump.

From these results, the useful Head and NPSHr curves are constructed in Fig. 10 with the objective of being able to verify the CFD modeling of the system under study and to be able to perform a DOE.

Fig. 10.a shows that the results obtained from the simulation show an error of less than 3. 5% when compared to the pump characteristic curve obtained experimentally. The closeness between these values shows the reliability of the experimental data. Additionally, Fig. 10.b shows the comparison of the simulated and experimental NPSHr. For the NPSHr, an error of less than 4% is observed when compared with the experimental results. Both curves (TDH and NPSHr) show a reduction as the pump flow increases, which is in accordance with the normal behavior of the pump.

The comparative results can be seen in Table 6, errors attributed to the data, is 3.5% less and 6.8% greater.

5. Design of experiment (DOE)

An experimental methodology design has been made available to reduce the time and cost required to analyze the operational points of Rio Magdalena dredge. In this order, the CCD algorithm or better known as Box-Vilson allows a limit of 20 entries [38], to have a great prediction in the corners of the design space [35]. Thus, the model based on this type of DOE allows adjusting linear and iteration effects, from the most influential variables of the operation of the dredge and adapt the results in regions or complex operating points. An optimal CCD design was sought to minimize both the degree of non-orthogonality and the autocorrelation of the input parameters of the coefficients, as well as the possibility that the sampling or validated points have an abnormal influence [36].

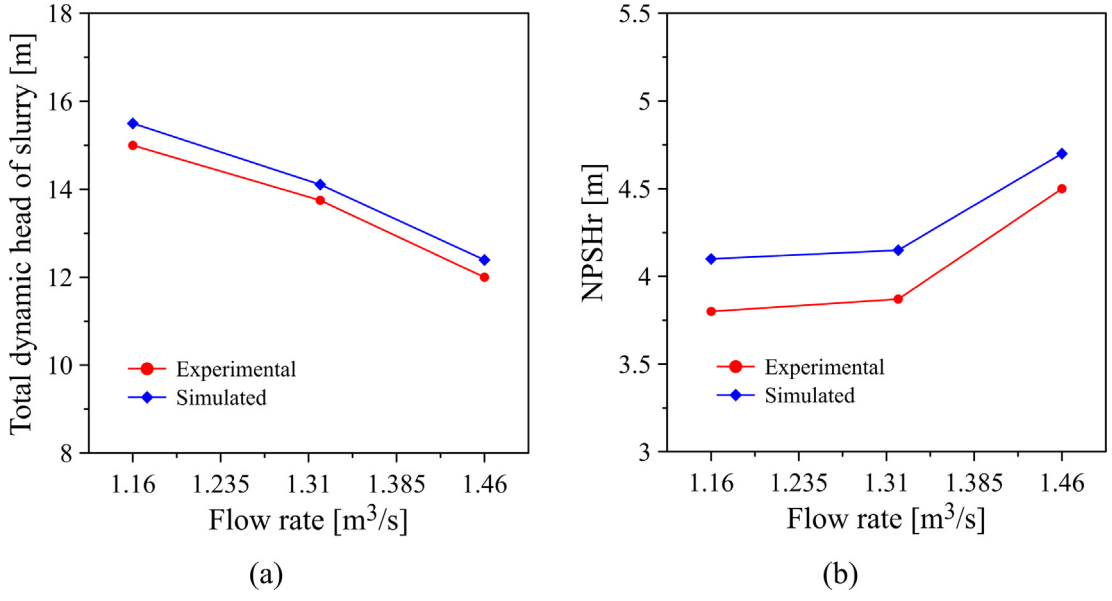

Fig. 10 Simulated versus experimental results for (a) Total dynamic head and (b) Net positive suction head required.

Table 6 Validation of the simulation with data taken in the field.

Test	Suction pressure [Pa]			Discharge pressure [Pa]		
	Experimental	Simulation	% Error	Experimental	Simulation	% Error
1	67727.80	71046.46	4.9	242502.57	254142.69	4.8
2	63568.61	66937.75	5.3	239330.55	246271.14	2.9
3	54182.20	56078.58	3.5	230135.13	239110.40	3.9

Table 7 Treatment levels and coded values of the independent variables or factors used in the characterization of the cavitation phenomenon.

Values					
Factors	Low −1	Centered 0	High 1	Units	Continuous
RPM	201.14	215.52	229.90	rev/min	Yes
Swing speed	0.10	0.24	0.37	m/s	Yes
Density	1.20	1.40	1.60	ton/m^3	Yes
Depth of dredging	0.00	6.35	12.70	m/	Yes
Slurry velocity at the discharge	4.00	5.00	6.00	m/s	Yes

Table 8 Results of central rotary composite experiment design.

DOE	Dependent or Input variables					Independent or Objective variables	
	Swing speed [m/s]	RPM	Density [ton/m^3]	Depth of dredging [m]	Fluid speed [m/s]	Suction pressure [Pa]	Discharge pressure [Pa]
1	0.23	215.52	1.40	6.35	5.00	50452.26	241578.51
2	0.10	215.52	1.40	6.35	5.00	50403.72	239927.97
3	0.36	215.52	1.40	6.35	5.00	50516.16	238599.06
4	0.23	201.14	1.40	6.35	5.00	50452.26	239441.02
5	0.23	229.9	1.40	6.35	5.00	50452.27	239976.06
6	0.23	215.52	1.20	6.35	5.00	60982.99	247750.02
7	0.23	215.52	1.60	6.35	5.00	42563.39	233781.25
8	0.23	215.52	1.40	0.00	5.00	12553.99	178965.23
9	0.23	215.52	1.40	12.71	5.00	113458.51	302400.27
10	0.23	215.52	1.40	6.35	4.00	50452.26	241727.75
11	0.23	215.52	1.40	6.35	6.00	50452.26	241720.21
12	0.17	208.33	1.30	3.17	5.50	21352.95	210541.91
13	0.30	208.33	1.30	3.17	4.50	21418.94	215400.2
14	0.16	222.71	1.30	3.17	4.50	21352.95	211145.57
15	0.30	222.71	1.30	3.17	5.50	21418.95	212941.05
16	0.17	208.33	1.50	3.17	4.50	16817.89	205495.33
17	0.30	208.33	1.50	3.17	5.50	16868.62	208520.89
18	0.17	222.71	1.50	3.17	5.50	16817.89	206652.39
19	0.30	222.71	1.50	3.17	4.50	16868.62	215980.61
20	0.17	208.33	1.30	9.52	4.50	89205.75	275381.75
21	0.30	208.33	1.30	9.52	5.50	89271.56	285412.42
22	0.17	222.71	1.30	9.52	5.50	89205.75	276781.10
23	0.30	222.71	1.30	9.52	4.50	89271.56	280415.91
24	0.17	208.33	1.50	9.52	5.50	75623.73	265015.12
25	0.30	208.33	1.50	9.52	4.50	75674.46	264965.27
26	0.17	222.71	1.50	9.52	4.50	75623.73	266200.63
27	0.30	222.71	1.50	9.52	5.50	75674.46	269750.45

Table 9 ANOVA for lineal multiple regression.

Variance Analysis					
Degree of freedom		Sum of squares	Square average	F	P-value
Regression	2	21410549552.87	10705274776.43	440.65	1.21E−19
Residual	24	583063478.57	24294311.61		
Total	26	21993613031.44			

If N is the number of input parameters, a fractionated central composite design based on a central composite design consists of a central point, 2n point of the axis at the position y on each axis of the selected input parameters and factorial points located at and along the diagonals of the input parameter space.

Table 10 Statistic for the multiple linear regression.

Regression Statistics	
Pearson coefficient	0.986
Square Pearson R^2	0.973
Adjusted R^2	0.971
Error	4928.926
Sample size	27

For the present case, five input parameters are considered: swing velocity, pump revolutions per minute, dredging depth, mixing density, and slurry velocity at the discharge of the pump. The factors considered are presented in Table 7, and the calculation of the points required for the analysis is obtained using Eq. (19)

$$N = 2^{n-f} + 2 \cdot n + c = 2^{5-1} + 2 \cdot (5) + 1 = 27 \tag{20}$$

That is, 27 simulations are required to perform the DOE study and thus have knowledge of the behavior of the system throughout its range of variation.

The points or expanded data spectrum are calculated in the Design Explorer algorithm to the responses obtained from the objective variables presented in Table 8.

6. Results and discussion

With the results obtained from the experimental design carried out, a multiple linear regression was implemented with the form shown in Eq. (21) [37]. The results allowed to analyze the influence and obtain the significant input variables that affect the dependent or objective variables such as suction and discharge pressure.

$$\mu|x_1, x_2, x_3, \cdots, x_n| = \beta_0 + \beta_1 x_1 + \beta_2 x_2 + \cdots + \beta_k x_k \tag{21}$$

From the variables presented in Table 7 and the suction pressure values obtained, a hypothesis test was performed to determine the actual variables influencing the model. An ANOVA was used to assess the model's ability.

The final model, shown in (22), was obtained using the following set of variables: suction pressure as a predicted variable, working fluid density, and dredging independent depth as independent variables.

$$P_s = 96314.6 - 24216.2 \cdot \rho_{md} - 5214.4 \cdot Z_1 \tag{22}$$

The ANOVA analysis of the model is shown in Table 9. The Fisher test applied to the regression rejected the null hypothesis.

Therefore, the coefficients obtained are significant for the regression at a 95% confidence level. The statistical results of the regression are shown in Table 10.

It is observed that 97.34% of the variance of the model is explained by the dependent variables used. Therefore, this model has an excellent predictive capacity. Furthermore, the adjusted R^2 was checked, and it was found that the variables used in the model are very influential.

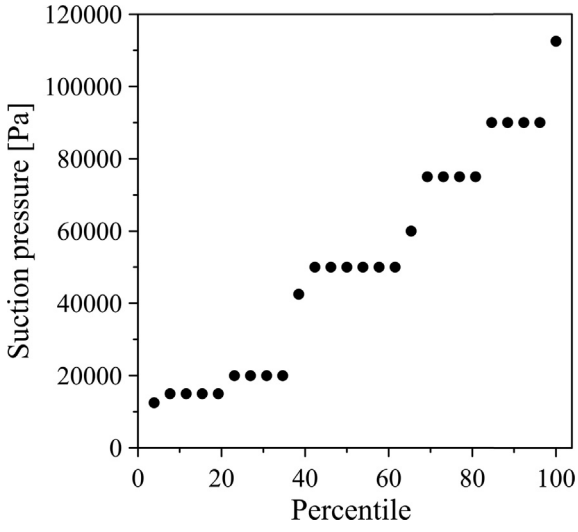

Fig. 12 Normal probability for the sample used on the multiple linear regression for suction pressure.

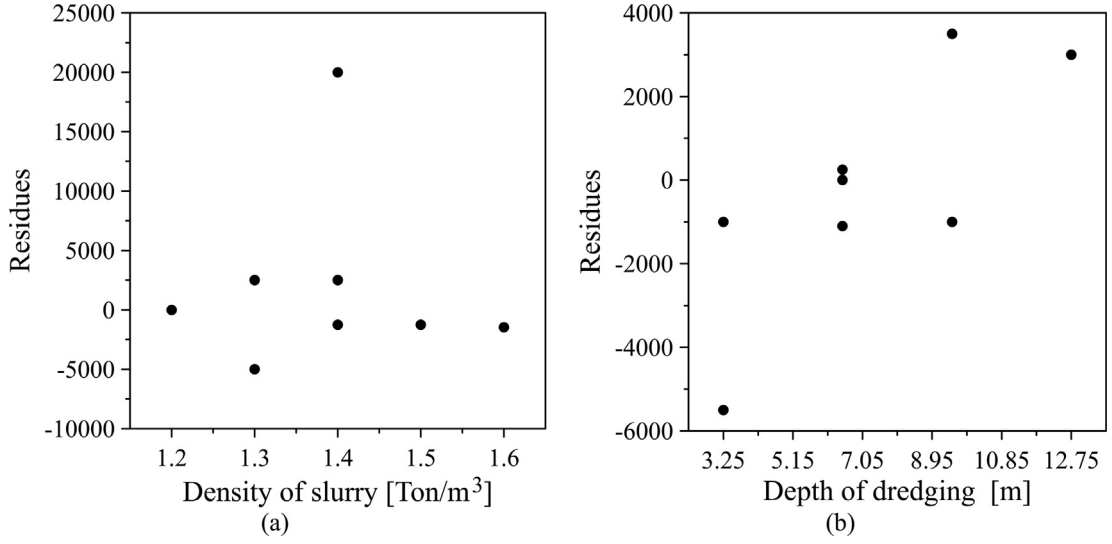

Fig. 11 Adjusted residuals graphic for suction pressure: (a) density of slurry and (b) depth of dredging.

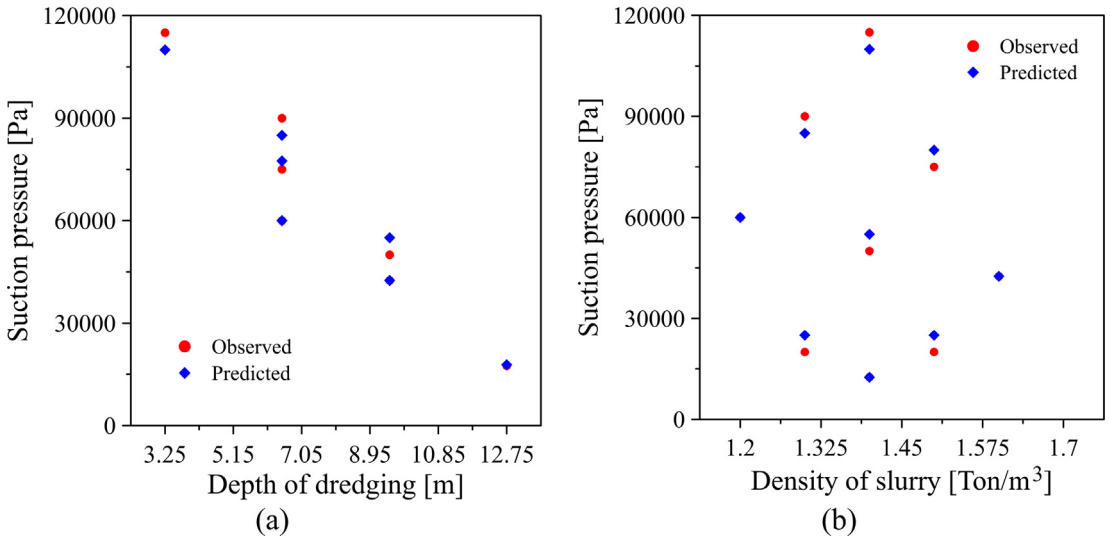

Fig. 13 Predicted values and real values for the correction factor versus the variables influencing the model for suction pressure: (a) depth of dredging and (b) density of slurry.

Table 11 ANOVA for lineal multiple regression.

Variance Analysis					
Degree of freedom		Sum of squares	Square average	F	P-value
Regression	2	23434413653.02	11717206827.04	1026.157	5.688E−24
Residual	24	274044681.10	11418528.38		
Total	26	23708458334.21			

Table 12 Statistic for the multiple linear regression.

Regression Statistics	
Pearson coefficient	0.994
Square Pearson R^2	0.988
Adjusted R^2	0.987
Error	3379.131
Sample size	27

It has performed a residual analysis that is illustrated in Fig. 11. It shows how the residuals vary respect to the dependent variables of the model. It is noticed that there are no erratic patterns that can infer interdependence or causal relationship in the independent variable, an inappropriate model, or inequalities.

The residuals presented suitable randomness around 0 (zero), which confirms the adequacy of the independent variables in the model. Also, the normal probability plot of the sample, shown in Fig. 12, has a good linear trend. It confirms that the sample comes from a normal distribution, which is one of the assumptions used in the regression model.

Fig. 13 presents the capability of the model to predict the suction pressure depending on the relevant variables of the model.

The final model, shown in Eq. (23), was obtained using the following set of variables: discharge pressure as a predicted variable, working fluid density, and dredging depth as independent variables.

$$Pd = 233810.9 - 38907.0 \cdot \rho_{md} + 9765.285 \cdot z_1 \quad (23)$$

The ANOVA analysis of the model is shown in Table 11. The Fisher test is used to reject the null hypothesis. Therefore, the coefficients obtained are significant for the regression at a 95% confidence level. The residuals presented suitable randomness around 0 (zero), which confirms the adequacy of the independent variables in the model. The results of the regression are shown in Table 12.

It is observed that 98.84% of the variance of the model is explained by the dependent variables used. Therefore, this model has excellent predictive capacity.

Fig. 14 shows how the residuals vary according to the dependent variables used in the model. It is observed that there are no unusual patterns that may infer interdependence or causal relationship in the independent variable, an inappropriate model, or inequalities. The residuals presented suitable randomness around 0 (zero), which confirms the adequacy of the independent variables in the model.

Also, the normal probability plot of the sample, shown in Fig. 15, has a good linear trend. This allows concluding that the sample comes from a normal distribution, which is one of the assumptions used in the regression model.

To evaluate the predictive capacity of the model, the predicted and experimental discharge pressure is presented in

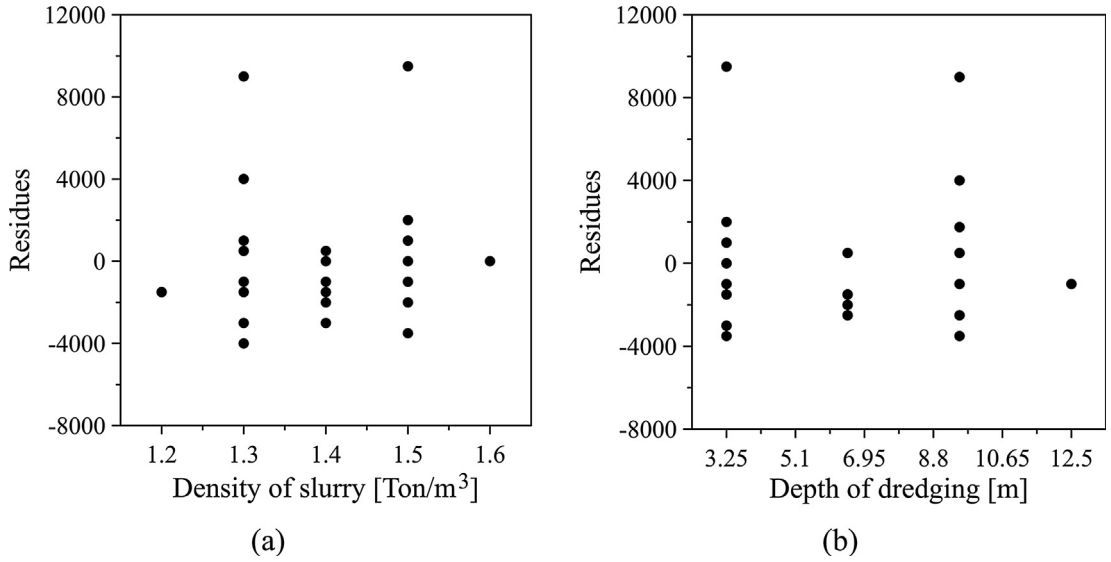

Fig. 14 Adjusted residuals graphic for discharge pressure: (a) density of slurry and (b) depth of dredging.

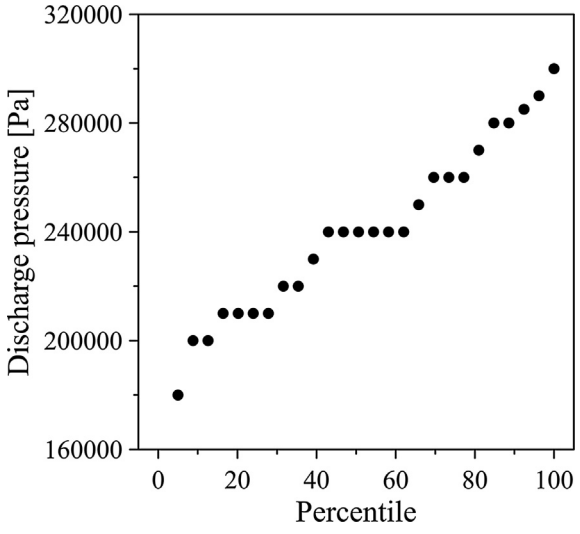

Fig. 15 Normal probability for the sample used in the multiple linear regression for discharge pressure.

Fig. 16, and it is observed a good predictive ability. For statistical principle, the regressions obtained are only valid for the range of operations that were considered during the investigation. This behavior is consistent with that observed in Fig. 8, and it is due to increasing the depth of dredging and the density of the slurry, an increase occurs in the kinetic turbulence energy of the fluid, thus increasing the energy needed to move the slurry into the pump.

Similarly, the chosen turbulence model was able to predict the cavitation phenomenon in the CFD process. Fig. 17 shows the predicted values, and they are very close to the experimental data. This graphically highlights the predictive ability of the proposed fitted model in the proposed operating ranges.

Fig. 17.a shows an increasing behavior of NPSHr with increasing slurry density. This is due to the pressure drop caused by the increase in slurry density, as shown in Figs. 7c and 8c. This reduction of pressure in the suction and discharge of the pump implies a reduction of the pressure levels inside the pump. Research such as those by Zhao and Zhao [40] describe similar results.

Fig. 17b, independence of the NPSHr with respect to the dredging depth, was observed. Which is in accordance with the normal behavior of the pump, since a change in dredging depth is expected to only affect the NPSH available. Additionally, the mathematical model of the NPSHr of Karassik et al. [41] shows that this only changes with an increase in the flow rate or a change in the rotation speed of the pump. Neither of these two parameters is influenced by dredging depth.

The rationale for understanding the problems in the suction line is the key to the present characterization. Most problems with the hydraulic transport system are originated in the suction line due to the limitation presented by atmospheric pressure; its equilibrium tends to be altered. In a dredging pump, the only force that overcomes the loss of the suction line is atmospheric pressure.

A conventional dredging pump operates with 24.71 in Hg at the pump feed during operations; it represents vacuum in the suction line or 5.9 in Hg absolute pressure. If the operator exceeds the vacuum of 24.71 in Hg, he runs the risk of suffering from the cavitation phenomenon [38]. Fig. 18 shows the decompensation of the admissible vacuum the pump can withstand while dredging by increasing the net positive suction head requerid.

Fig. 18 can be adjusted to a mathematical model of the form:

$$\mathrm{VACUUM}_{admissible} = 30.01 - 4.02 \cdot \mathrm{NPSH}_r \tag{24}$$

This implies that when the NPSHr is increased, the pump loses suction capacity, which is represented by a reduction in dredging efficiency (amount of slurry pumped).

Despite the results obtained, the modeling conditions have high computational requirements. Because of this, the computational effort was strengthened considering an experimental design that would reproduce the most relevant operating areas

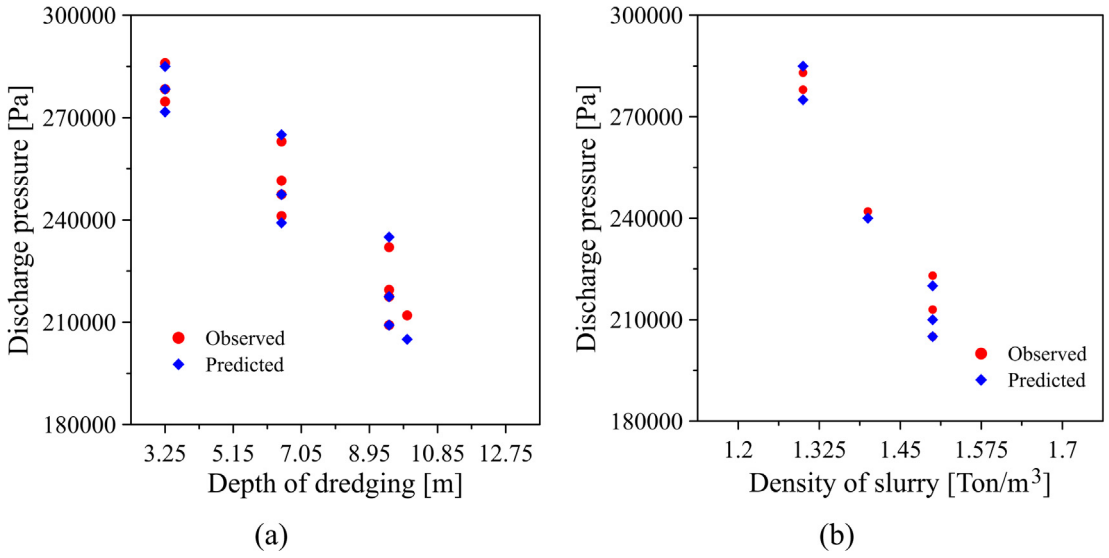

Fig. 16 Predicted values and real values for the correction factor versus the variables influencing the model for discharge pressure: (a) depth of dredging and (b) density of slurry.

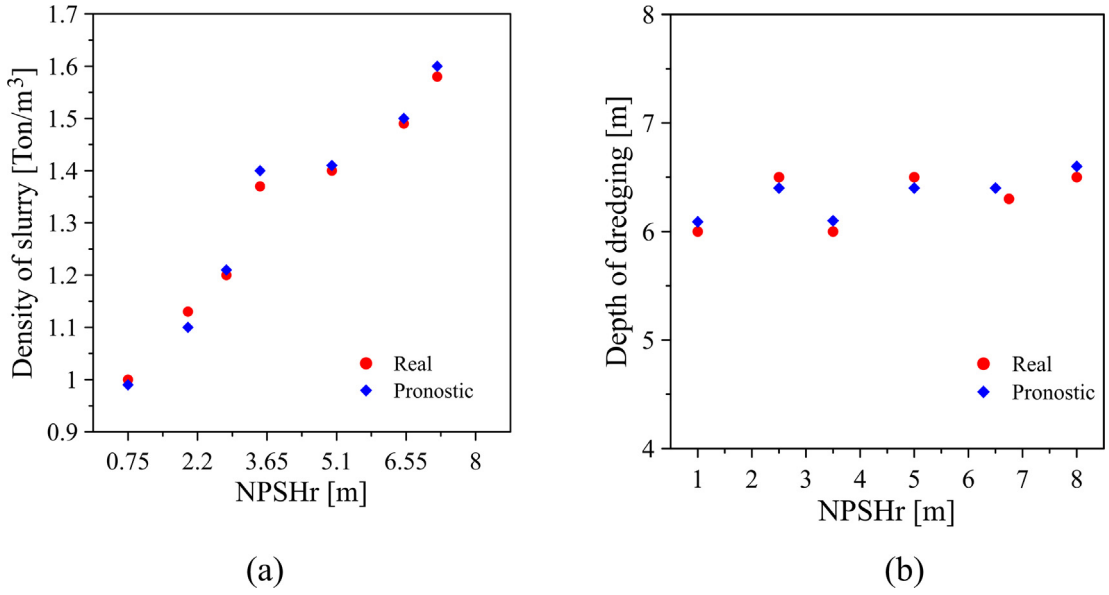

Fig. 17 Comparison of the actual values of NPSHr versus the predictions for NPSHr of the adjusted model: (a) density of slurry and (b) depth of dredging.

during dredging. This process was accompanied by mesh independence analysis. As stipulated in the physical definition, the particle model was coupled using mean grain size d_{50} = 0.169 mm [37].

To characterize and mitigate the cavitation phenomenon under the parameters and expressions previously obtained for the centrifugal pump, an analysis of the capacity of the pump is established.

The importance of the present characterization lies in the possibility of being able to identify the limitations of a system being affected by cavitation. However, when observing the influence of the simulations and performing the previous analyzes, it is emphasized that only the variables that significantly influence the process are dredging depth and slurry density, which in turn is influenced by the strong presence of stationary sandbanks or mud in the suction pipe. It is important to clarify that this model is only valid for the operational range observed in Table 13.

To develop a model capable of characterizing the cavitation phenomenon of the centrifugal dredging, under different operating conditions and type of slurry.

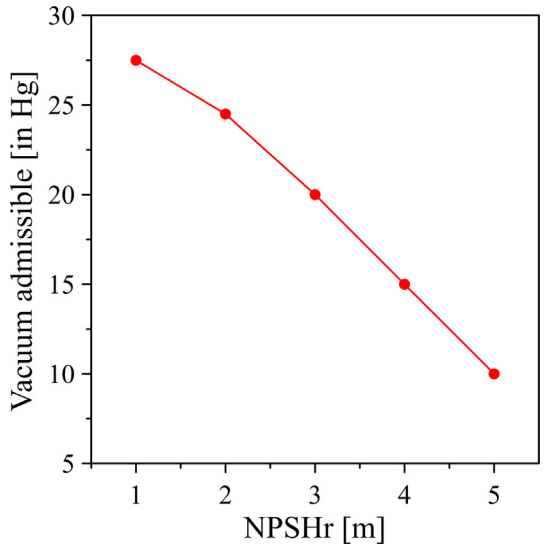

Fig. 18 Vacuum admissible as a function of the $NPSH_r$.

Table 13 Correlations and limitations.

Correlations	Limitations
$P_s = 96314.6 - 24216.2 \cdot \rho_{md} - 5214.4 \cdot Z_1$	ρ_{md} : 1.2–1.6 [ton/m^3]; Z_1: 0–12.7 [m]
$Pd = 233810.9 - 38907.0 \cdot \rho_{md} + 9765.285 \cdot Z_1$	ρ_{md} : 1.2–1.6 [ton/m^3]; Z_1: 0–12.7 [m]
$TDH = \frac{177375.3+6663.1 \cdot \rho_{md}+468.12 \cdot Z_1}{\rho_{md} \cdot g \cdot 1000}$	ρ_{md} : 1.2–1.6 [ton/m^3]; Z_1: 0–12.7 [m]
$VACUUM_{admissible} = 30.01 - 4.02 \cdot NPSH_r$	$NPSH_r$: 0–6 [m]

7. Conclusions

As a result of this investigation, it was possible to develop a series of correlations that defends the hydraulic behavior of the pump applied to the dredging industry. It is of the utmost importance to take into account the parameters described by the equations in Table 13. The use of these correlations allows mitigating the negative effects of cavitation on the pump, and the characterization was mainly based on the recognition of the conditions of operation where a critical vacuum pressure was avoided. For the case under study, it was determined that if the vacuum pressure was below 5.9 in Hg, cavitation was presented for the operating temperature. If this condition occurs, the vapor bubbles that would form would travel to areas of greater pressure inside the pump housing, would imply and lead to internal erosion, affecting not only the hydraulic performance but also its durability.

The influences of the dredged site for the characterization of the process were factors that impacted the study. As a general characteristic, for a typical year, the Calamar sector – Colombia has low water levels, between February and April, high water levels, from October to December and intermediate levels, the rest of the year. In order to standardize the simulation process, mean grain size d_{50} = 0.169 mm was used, taking into account the measurements in Calamar sector [33]. The swing velocity has an impact on the performance of the pump due to the pressure changes created by the pipe motion. The relative velocity between water and the pipe entry can increase or decrease the pressure drop coefficient, and this creates situations where cavitation can be promoted. Furthermore, the eddies created behind the pipe due to the motion, at certain moments will create a lower pressure condition around the inlet, and the effect will bet transferred along the inlet pipe. At the moment the Eddie is dissipated, the pressure will increase, creating a new condition where pressure increases.

To check the influence of geometric considerations and increase the necessary data, a methodology was structured in a CFD software considering stages, where an intense simulation activity was based on trial and error. CFD-DOE was carried out to validate the performance characteristics of the dredging pump, and to verify the presence of the cavitation phenomenon. The complex field of the internal flows of the pump was investigated by using the criteria offered by CFD, allowing significant control of the numerical methods used in the software and the types of meshes required for the fluid domains within the pipe, the volute, and the impeller (Fig. 4). For this reason, the comparisons of the useful head and the NPSHr obtained at the simulated operating points showed great agreement with the turbulence model RNG k-ε, the Eulerian-Lagrangian approach for multiphase flows and finally the cavitation model based on the equation of Rayleigh-Plesset (RP). Mesh independence was guaranteed in the present study (Fig. 5). This leads to the results of the order of 4% (Fig. 10), which verifies the high capacity of the developed model.

Fig. 6 shows the effect of slurry on the hydraulic performance of the pump. It is noted that the presence of Slurry decreases the pump head to the same as the presence of cavitation, because part of the energy delivered in the impeller dissipates due to the phase change in the liquid, which is consistent with the work of Li et al. [39].

Figs. 7 and 8 show the influence of different analysis variables on the suction and discharge pressure of the pump. It is observed that the increase in density results in a decrease in pump suction and discharge pressure. Additionally, the increase in the number of solid particles in the fluid causes an increase in the kinetic turbulence energy of the fluid, thus increasing the energy needed to pump the slurry into the pump. In the case of the swing speed and the rpm of the pump, when these parameters are increased, it is observed that the suction pressure as the discharge pressure is also increased.

The application of statistical tools such as DOE and multiple linear regressions showed excellent results regarding the significant and theoretical statistics of the previously established CFD methodology. For this, all the validations applied to the expressions obtained to quantify the useful head, the admissible NPSH, and the maximum vacuum allowed, presented excellent results (Figs. 11–17). This is translated into a model able to predict the cavitation phenomenon in the dredging pump and a way to mitigate the phenomenon.

The cavitation phenomenon can negatively affect the performance of the Rio Magdalena dredge. The current characterization allows operating within the capabilities of this predictive model. It also recognizes the capacity of a pump in a cut-type dredger and the vacuum created.

Declaration of Competing Interest

The authors declared that there is no conflict of interest.

Acknowledgments

- The authors thank the UNIVERSIDAD DEL ATLÁNTICO, SPHERE ENERGY Company, and DRAGADOS HIDRAULICOS S.A Company with the technical staff of the Rio Magdalena dredger for their support on the development of this research by allowing the use of its facilities and the required instrumentation.
- The authors thank the support provided by Colombian Institute for Scientific and Technological Development (COLCIENCIAS) through the "Convocatoria Nacional para Estudios de Doctorado en Colombia año 2012".

References

[1] S.A. Miedema, A head loss model for slurry transport in the heterogeneous regime, Ocean Eng. 106 (2015) 360–370, https://doi.org/10.1016/j.oceaneng.2015.07.015.

[2] J. Tang, Q. Wang, Z. Bi, Expert system for operation optimization and control of cutter suction dredger, Expert Syst. Appl. 34 (2) (2008) 2180–2192, https://doi.org/10.1016/j.eswa.2007.02.025.

[3] J. Tang, Q. Wang, T. Zhong, Automatic monitoring and control of cutter suction dredger, Autom. Constr. 18 (2) (2009) 194–203, https://doi.org/10.1016/j.autcon.2008.07.006.

[4] J. Tang, Q. Wang, Online fault diagnosis and prevention expert system for dredgers, Expert Syst. Appl. 34 (1) (2008) 511–521, https://doi.org/10.1016/j.eswa.2006.09.032.

[5] S. Chandel, S.N. Singh, V. Seshadri, A comparative study on the performance characteristics of centrifugal and progressive cavity slurry pumps with high concentration fly ash slurries, Part. Sci. Technol. 29 (4) (2011) 378–396, https://doi.org/10.1080/02726351.2010.503264.

[6] C. Camargo, C. García, J.E. Duarte Forero, A. Rincón, Modelo estadístico para la caracterización y optimización en bombas periféricas, Revista Científica Ingeniería y Desarrollo 36 (1) (2017) 18–39, https://doi.org/10.14482/inde.36.1.10939.

[7] M.C. Roco, G.R. Addie, R. Visintainer, Study on casing performances in centrifugal slurry pumps, Part. Sci. Technol. 3 (1) (1985) 65–88, https://doi.org/10.1080/02726358508906428.

[8] K.C. Wilson, R. Clift, A. Sellgren, Operating points for pipelines carrying concentrated heterogeneous slurries, Powder Technol. 123 (1) (2002) 19–24, https://doi.org/10.1016/S0032-5910(01)00423-5.

[9] S.R. Shah, S.V. Jain, R.N. Patel, V.J. Lakhera, CFD for centrifugal pumps: a review of the state-of-the-art, Procedia Eng. 51 (2013) 715–720, https://doi.org/10.1016/j.proeng.2013.01.102.

[10] Z.F. Yao, Z.J. Yang, F.J. Wang, Evaluation of near-wall solution approaches for large-eddy simulations of flow in a centrifugal pump impeller, Eng. Appl. Comput. Fluid Mech. 10 (1) (2016) 452–465, https://doi.org/10.1080/19942060.2016.1189362.

[11] X.W. Luo, J.I. Bin, Y. Tsujimoto, A review of cavitation in hydraulic machinery, J. Hydrodyn. Ser. B 28 (3) (2016) 335–358, https://doi.org/10.1016/S1001-6058(16)60638-8.

[12] Z.H.U. Bing, H.X. Chen, Cavitating suppression of low specific speed centrifugal pump with gap drainage blades, J. Hydrodyn. Ser. B 24 (5) (2012) 729–736, https://doi.org/10.1016/S1001-6058(11)60297-7.

[13] A. Peters, H. Sagar, U. Lantermann, O. el Moctar, Numerical modelling and prediction of cavitation erosion, Wear 338 (2015) 189–201, https://doi.org/10.1016/j.wear.2015.06.009.

[14] X.P. Long, Q.Q. Wang, L.Z. Xiao, J.Q. Zhang, M.S. Xu, W.F. Wu, B. Ji, Numerical analysis of bubble dynamics in the diffuser of a jet pump under variable ambient pressure, J. Hydrodyn. Ser. B 29 (3) (2017) 510–519, https://doi.org/10.1016/S1001-6058(16)60763-1.

[15] H. Liu, Y. Wang, D. Liu, S. Yuan, J. Wang, Assessment of a turbulence model for numerical predictions of sheet-cavitating flows in centrifugal pumps, J. Mech. Sci. Technol. 27 (9) (2013) 2743–2750, https://doi.org/10.1007/s12206-013-0720-8.

[16] X. Long, H. Cheng, B. Ji, R.E. Arndt, X. Peng, Large eddy simulation and Euler-Lagrangian coupling investigation of the transient cavitating turbulent flow around a twisted hydrofoil, Int. J. Multiph. Flow 100 (2018) 41–56, https://doi.org/10.1016/j.ijmultiphaseflow.2017.12.002.

[17] F. Bakir, R. Rey, A.G. Gerber, T. Belamri, B. Hutchinson, Numerical and experimental investigations of the cavitating behavior of an inducer, Int. J. Rotating Mach. 10 (1) (2004) 15–25, https://doi.org/10.1155/S1023621X04000028.

[18] P. Limbach, R. Skoda, Numerical and experimental analysis of cavitating flow in a low specific speed centrifugal pump with different surface roughness, ASME J. Fluids Eng. 139 (10) (2017) 101201, https://doi.org/10.1115/1.4036673.

[19] F. Zhang, S. Yuan, Q. Fu, J. Pei, M. Böhle, X. Jiang, Cavitation-induced unsteady flow characteristics in the first stage of a centrifugal charging pump, ASME J. Fluids Eng. 139 (1) (2017) 011303, https://doi.org/10.1115/1.4034362.

[20] D.S. Zhang, W.D. Shi, G.J. Zhang, J. Chen, B.B. van Esch, Numerical analysis of cavitation shedding flow around a three-dimensional hydrofoil using an improved filter-based model, J. Hydrodyn. Ser. B 29 (2) (2017) 361–375, https://doi.org/10.1016/S1001-6058(16)60746-1.

[21] Y. Wang, H. Liu, D. Liu, S. Yuan, J. Wang, L. Jiang, Application of the two-phase three-component computational model to predict cavitating flow in a centrifugal pump and its validation, Comput. Fluids 131 (2016) 142–150, https://doi.org/10.1016/j.compfluid.2016.03.022.

[22] H.L. Liu, D.X. Liu, Y. Wang, X.F. Wu, J. Wang, Application of modified κ-ω model to predicting cavitating flow in centrifugal pump, Water Sci. Eng. 6 (3) (2013) 331–339, https://doi.org/10.3882/j.issn.1674-2370.2013.03.009.

[23] H. Si, Y. Fuxiang, G. Jing, Numerical simulation of 3D unsteady flow in centrifugal pump by dynamic mesh technique, Procedia Eng. 61 (2013) 270–275, https://doi.org/10.1016/j.proeng.2013.08.015.

[24] O. Coutier-Delgosha, R. Fortes-Patella, J.L. Reboud, M. Hofmann, B. Stoffel, Experimental and numerical studies in a centrifugal pump with two-dimensional curved blades in cavitating condition, ASME J. Fluids Eng. 125 (6) (2003) 970–978, https://doi.org/10.1115/1.1596238.

[25] W.G. Li, Modeling viscous oil cavitating flow in a centrifugal pump, ASME J. Fluids Eng. 138 (1) (2016) 011303, https://doi.org/10.1115/1.4031061.

[26] A.A. Babajani, M. Jafari, P.H. Sefat, Numerical investigation of distance effect between two Searasers for hydrodynamic performance, Alex. Eng. J. 55 (3) (2016) 2257–2268, https://doi.org/10.1016/j.aej.2016.05.022.

[27] D.A. Wilson, Pipeline dredge analytical program with comparison to field data, J. Pipeline Syst. Eng. Pract. 2 (3) (2011) 107–112, https://doi.org/10.1061/(ASCE)PS.1949-1204.0000078.

[28] S.A. Miedema, An analysis of slurry transport at low line speeds, in: ASME 33rd International Conference on Ocean, Offshore and Arctic Engineering, OMAE2014-23437, 2014, https://doi.org/10.1115/OMAE2014-23437.

[29] J. Capecelatro, O. Desjardins, Eulerian-Lagrangian modeling of turbulent liquid–solid slurries in horizontal pipes, Int. J. Multiph. Flow 55 (2013) 64–79, https://doi.org/10.1016/j.ijmultiphaseflow.2013.04.006.
[30] M.K. Gopaliya, D.R. Kaushal, Analysis of effect of grain size on various parameters of slurry flow through pipeline using CFD, Part. Sci. Technol. 33 (4) (2015) 369–384, https://doi.org/10.1080/02726351.2014.971988.
[31] D.R. Kaushal, T. Thinglas, Y. Tomita, S. Kuchii, H. Tsukamoto, CFD modeling for pipeline flow of fine particles at high concentration, Int. J. Multiph. Flow 43 (2012) 85–100, https://doi.org/10.1016/j.ijmultiphaseflow.2012.03.005.
[32] Cormagdalena, Actualización del PMA de los dragados de relimpia y mantenimiento del Canal del Dique, Barranquilla, 2004.
[33] I. Quintero, Estudio del Transporte de Sedimentos en el Río Grande de la Magdalena: Canal de acceso al Puerto de Barranquilla, Doctoral dissertation, Universidad Nacional Autónoma de México, 2015.
[34] A.K. Singhal, M.M. Athavale, H. Li, Y. Jiang, Mathematical basis and validation of the full cavitation model, J. Fluids Eng. 124 (3) (2002) 617–624, https://doi.org/10.1115/1.1486223.
[35] G. Fu, A. Untaroiu, An optimum design approach for textured thrust bearing with elliptical-shape dimples using computational fluid dynamics and design of experiments including cavitation, J. Eng. Gas Turbines Power 139 (9) (2017) 092502, https://doi.org/10.1115/1.4036188.
[36] D.C. Montgomery, Design and Analysis of Experiments, John Wiley & Sons, 2017.
[37] M. Bilgili, B. Sahin, Comparative analysis of regression and artificial neural network models for wind speed prediction, Meteorol. Atmos. Phys. 109 (1) (2010) 61–72, https://doi.org/10.1007/s00703-010-0093-9.
[38] D. Kang, K. Yokota, Analytical study of cavitation surge in a hydraulic system, J. Fluids Eng. 136 (10) (2014) 101103, https://doi.org/10.1115/1.4027220.
[39] Y. Li, Z. Zhu, W. He, Z. He, Numerical simulation and experimental research on the influence of solid-phase characteristics on centrifugal pump performance, Chin. J. Mech. Eng. 25 (6) (2012) 1184–1189, https://doi.org/10.3901/cjme.2012.06.1184.
[40] W. Zhao, G. Zhao, Numerical investigation on the transient characteristics of sediment-laden two-phase flow in a centrifugal pump, J. Mech. Sci. Technol. 32 (1) (2018) 167–176, https://doi.org/10.1007/s12206-017-1218-6.
[41] I.J. Karassik, J.P. Messina, P. Cooper, C.C. Heald, Pump Handbook, Vol. 3, McGraw-Hill, New York, 2001.